https://dx.doi.org/10.4314/dujopas.v9i4a.4
ISSN (Print): 2476-8316
ISSN (Online): 2635-3490
Dutse Journal of Pure and Applied Sciences (DUJOPAS), *Vol. 9 No. 4a December 2023*

Application of Integrated Geophysical Methods in Mapping the Location of Basaltic Intrusions in Mambilla Plateau and Environs, Northeast, Nigeria

Yohanna Andarawus[1]* Othniel Kamfani Likkason[2], Maigari Abubakar Sadiq[3], Ali Sani[2] Iyakwari Shekwonyadu[1] and Mohammed Kaura Aliyu[1]

[1]Department of Geology,
Federal University of Lafia, P.M.B 146,
Nasarawa State, Nigeria

[2]Department of Physics,
Abubakar Tafawa Balewa University Bauchi,
P.M.B 0248,
Bauchi State,
Nigeria

[3]Department of Applied Geology,
Abubakar Tafawa Balewa University Bauchi,
P.M.B 0248,
Bauchi State,
Nigeria

Email: sarkikubong@gmail.com, yohana.andarawus@science.fulafia.edu.ng

Abstract

Integrated geophysical investigation on the Mambilla Plateau and its environs was necessary to map the locations of basaltic intrusions and their patterns of distribution. The Landsat-8 ETM+ false colour composite image (bands 7, 4, 2 in R, G, and B) was used to identify rocks such as younger basalt (yb), porphyritic granite (pg), granite gneiss (Gn), and migmatite gneiss (Mg). Similarly, rocks like granite gneiss (Mg), porphyritic granite (pg), and migmatite gneiss (Mg) were recognised by the Principal Component Analysis of the Landsat 8 ETM+ picture (PC2, PC1, and PC4 in R, G, and B). The lowest and maximum values for the total magnetic intensity map were 33030.343 nT and 33172.792 nT, respectively, along with mean of value 31.50nT to 33068.89nT.The primary magnetic field map showed an average value of 33293.4495 nT, with values ranging from 33228.522nT to 33358.377nT. The crustal magnetic field map resulting from ore bodies or intrusions had an average value of -159.50 nT, with values ranging from -397.669 nT to -80.699 nT. The RTE values, which range from -82.382nT to -392.122nT, indicate regional geological intrusions, fractures, and faults. Values were shown on the magnetic equator field map, which was further upward continued to 15 km, with an average values ranging from -279.141nT to -157.160nT. The pseudo-gravity map of the region showed two low densities, ranging from -0.11 to -0.01 mGal, depending on the location, and three high densities, indicating moderate to intermediate densities, ranging from 0.25 mGal to 0.01 mGal. RTE anomaly data produced from subsurface rocks typically has the greatest horizontal gradient along the object's

*Author for Correspondence

border. This means that the maximum gradient is directly localised to the map boundaries of the distinct lithologies. By examination of the abrupt changes in rock magnetism in a lateral direction, this led to the determination of contact limits of the basaltic intrusion, faults, and mineralization of the underlying rocks.

Keywords: Intrusions, Basalts, Pseudogravity, Landsat, Aeromagnetic

INTRODUCTION

Geophysical methods have diverse applications in minerals, groundwater, hydrocarbon exploration and in geotechnical studies. In the field of mining geophysics magnetic and remote sensing methods are used in preliminary exploration of mining regions and for detailed studies of igneous intrusions, igneous dikes, and contact-metamorphic zones in relation to which various types of ores may occur. They are used to identify structural features, faults, contacts, shear zones, joints, promising mineralization sites and alteration zones (Eldosouky, 2019, Elkhateeb and Eldosouky, 2016).

However, lithological units, hydrothermal alteration zones, and structural features connected to various mineralizations have been mapped using satellite remote sensing imagery data (Pour and Hashim, 2016). To clearly define the hydrothermal alteration zones and possible mineralization locations, a number of enhancement techniques, including band ratios and Constrained Energy Minimization (CEM), are frequently used (Poormirzaee and Oskouei, 2010).

Extrusive igneous rocks make up basaltic rocks. These are volcanic rocks that formed on Earth's surface by the freezing of lava. In general, basaltic rocks are black in colour, relatively massive, and contain a small amount of silica and a lot of iron elements. Because of their high density and resistance to weathering, basaltic rocks are popular choices for building materials (Anonymous, 2020).

Since basaltic rock mining has started to boom, an attempt must be made to map the location and distribution of basaltic rock intrusion throughout the Mambilla Plateau and its surroundings in order to advise both domestic and foreign investors on basalts quarrying. The distribution of high density basaltic rocks, which are important as building materials, can be found with the help of this research. A magnetic survey is one geophysical method that can be used to map basaltic rocks in a region, along with other methods like landsat (Adagunodo *et al*., 2015).

Despite being beneath, basaltic rocks can be easily recognised owing to the great sensitivity of the magnetic survey, which can identify and map the distribution of basaltic rocks (Lino *et al*., 2018). The iron mineral content in the body of the rock is related to this, as it is typically ferromagnetic (Cyprian, 2016). Magnetic surveying offers various benefits in terms of data processing and interpretation. One benefit is the availability of a variety of magnetic anomalies data filtering techniques, which make it simple to understand magnetic anomalous sources in the subsurface that serve as targets in both qualitative and quantitative ways (Ansari and Alamdar, 2009).

The geological data indicated the presence of basaltic intrusions in the form of sills and dykes (Asikin and Handoyo 1992). The distribution pattern of basaltic intrusion in the region suggests that this rock intrusion first surfaced in Maisamari town as a dyke. Forming a sill,

the intrusions moved westward, into Ngoroje Village and the adjacent area. Therefore, the goal of this research is to use integrated geophysical approaches to determine the location of these intrusions. in order to help government create laws pertaining to basalt mining both now and in the future, especially the supply of pertinent data.

STUDY AREA LOCATION, GEOLOGICAL SETTING, AND GEOMORPHOLOGY

The study area is located in Taraba State, Northeastern Nigeria, and is part of the Sardauna and Gashaka Local Government Areas. It comprises the southernmost tip of the eastern half of the northern region of Nigeria and is situated between latitudes 6°30' 00''N and 7°30' 00''N and longitudes 11° 00' 00 E and 11° 30' 00''E. Its total land mass is 6,050 km² (Tukur *et al*., 2005). (Figure 1). The southern, eastern, and western portions of this plateau are locked with Cameroon (Frantz, 1981). More than two thirds of the plateau are under the Basement Complex rocks, which range from the Precambrian to the early Paleozoic epoch (Mubi and Tukur, 2005). In the meantime, volcanic rocks from the upper Cenozoic to Tertiary and Quaternary periods make up the remaining portion of the plateau and its surroundings (Jeje, 1983). The basaltic suite of volcanic rocks includes trachyte and olivine basalt. The plateau's eastern and southern escarpments are located along the Cameroonian border, while Nigeria controls the plateau's western slope and the remaining portion of its northern escarpment (Mould, 1960).

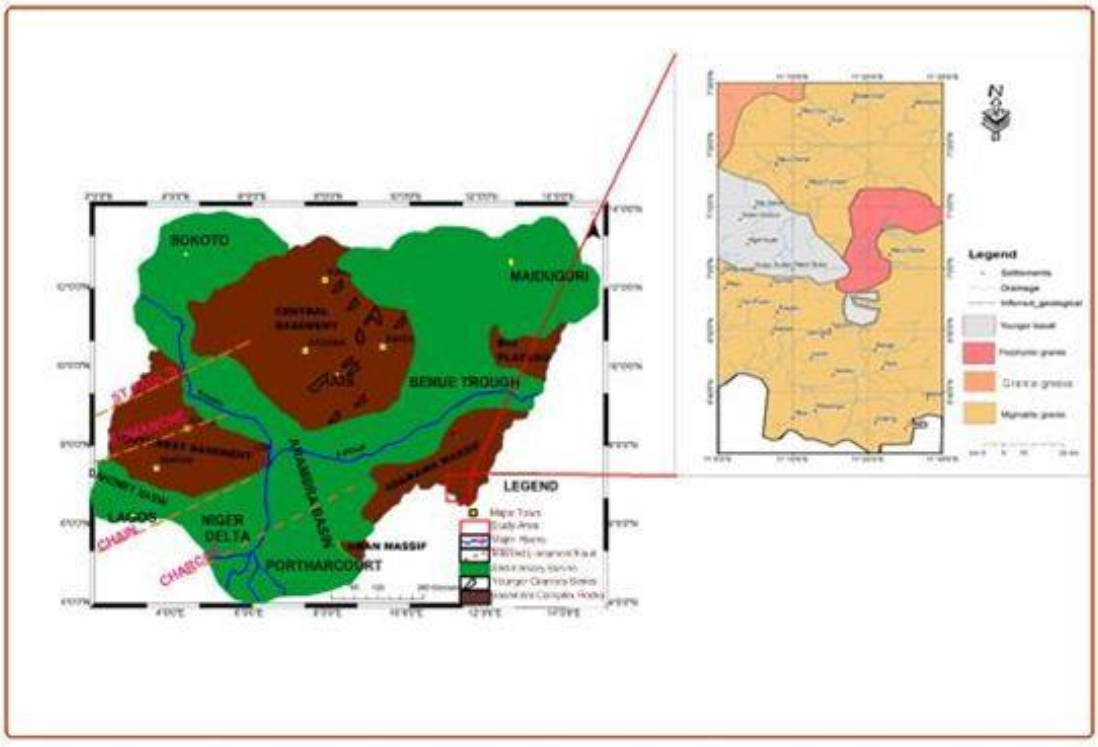

Figure 1: Structural map of Nigeria showing rocks distribution and the prominent fracture zones in Nigeria (Modified after Udensi *et al*., 2003).

MATERIALS AND METHODS

Remote Sensing Imagery Data

Two Landsat-8 pictures taken on July 7th , 2020, and September 30, 2020 were used. The Operational Land Imager (OLI) sensors are present in them (Roy et al., 1998). The visible and shortwave infrared reflect 30 m spatial resolution, while OLI offers data from nine spectral

bands providing resolution imaging, ranging from 15 m for the panchromatic band to 100 m for the thermal infrared spectrums (http://earthexplorer.usgs.gov). Using ArcGIS 10.8.2 and ENVI 5.7 software, the acquired data were subjected to a number of preprocessing stages, including geometric projection, atmospheric correction, spatial resolution merging, and mosaic production approach.

Band Ratio (BR)

Based on the variations in the spectral signature of minerals and distinct rock units, the Band Ratio (BR) approach is crucial for differentiating between different rock units and clarifying hydrothermal alteration zones (Goetz *et al*., 1983). The BR approach is typically required in mineral or lithological mapping in order to improve the spectral response of the alteration minerals within the alteration zones based on each alteration mineral's unique absorption characteristics at particular wavelengths (Pour *et al*., 2019). As a result, by choosing the right ratios in the BR approach, OH-bearing minerals and iron oxides may be distinguished accurately, producing an RGB composite image that can be used to accomplish the desired results.

Constrained Energy Minimization (CEM)

All of the signals were processed using the Constrained Energy Minimization (CEM) technique (Farrand and Harsanyi, 1997, Harsanyi, 1993). CEM has grown in significance and is now one of the most popular methods in target abundance mapping. By treating all characteristics other than the target as the unknown background, this approach maximises the reaction of the target spectrum and suppresses all other features' responses. Depending on the spectral signature of the alteration minerals, it aids in the identification of alteration zones. The spectral signatures of the minerals used in this investigation were obtained via the USGS spectral library and processed using ENVI V.5.3 software.

SRTM DEM Data

A comprehensive high resolution digital topographic database of Earth, known as Digital Elevation Models (DEM), is produced by the multinational Shuttle Radar Topography Mission (SRTM) project (Nikolakopoulos *et al*., 2006). From the DEM data, surface lineaments can be automatically extracted (Süzen and Toprak, 1998). In order to create shaded relief pictures, which are helpful for surficial lineaments and fault extraction, automatic lineaments mapping utilising shaded SRTM DEM 90m data was employed (Ganas *et al*., 2005). For the shaded relief photos, lines are automatically extracted by (PCI Geomatica, 2015) with default values. After that, the output is manually modified to exclude any man-made features (buildings, roads, etc.) in order to enhance the agreement between the extracted lines and the geological characteristics.

Aeromagnetic Data

The magnetic data grids for sheets 276 (Gashaka) and 295 (Mambilla) were provided by the Nigerian Geological Survey Agency (NGSA), and Geosoft Oasis Montaj TM 8.4.2 software was used to process them. Aeromagnetic data was collected using a Scintrex CS3 Cesium Vapour magnetometer, which collects Total Magnetic Intensity (TMI) data at 0.001 nT resolution and samples at 0.1 s. The dataset was gathered at 5000 metres of height, elevation, and tie line spacing, respectively. Prior to being reduced to a format that has an obvious and direct relationship with subsurface geology, the gathered aeromagnetic data were preprocessed. Using methods like reduction to magnetic equator (RTE), regional/residual field matched filtering, first and second vertical derivatives, total horizontal derivative, analytical signal, and pseudo-gravity transform, as well as MAGMAP's step-by-step filtering

processing, the magnetic data from the combined map of Gashaka (sheet 276) and Mambilla (sheet 295) were enhanced (Okpoli and Eyitoyo, 2016).

Reduction to the Equator (RTE)

Reduction To the Equator (RTE) comprises two components: a phase component (Icos (I) cos (D-δ) and an amplitude component sin (I) . North-South characteristics may explode when descending to the equator from low latitudes because of the numerical inaccuracy (from the term of 0/0) in the amplitude correction (the sin (I) component), which is performed when (D-δ) is δ/2 (i.e., a magnetic east-west wave number). The amplitudes of near North-South features, which are expressed as follows in the Geosoft Oasis Montaj software, can be slightly undercorrected in order to lessen or remove this issue.

$$L(\theta) = \frac{[\sin(I) - i.\cos(I)\cos(D-\theta)]^2 x(-\cos^2)(D-\theta)}{[\sin^2(I\alpha) + \cos^2(I\alpha).\cos^2(D-\theta)]x[\sin^2(I) + \cos^2(I).\cos^2(D-\theta)]} \quad (1)$$

if ($|I\alpha| < |I|$), $I\alpha = I$

where: *I* geomagnetic inclination, Iα inclination for amplitude correction (never less than I), *D* geomagnetic declination.

Upward Continuation

It is useful for regional-residual separation because upward continuation attenuates the anomalies of shallow features and comparatively amplifies the anomalies of deeper sources. The shallow features known as the residual field are what remain after deducting the somewhat deeper sources from the total field (Tanaka *et al.*, 1999). The upward continuation filter's frequency response is provided as:

$$F_u(u, v, h) = e^{-2\pi h}(u^2 + v^2)^{1/2} \quad (2)$$

where *h* is the height to which the field is continued and "u" and "v" are equivalent of x and y coordinates in the frequency domain. Upward continuation may be applied to suppress the effects of small scale features near the surface (Telford *et al.*, 1990). It is also used to reduce topographic effects. For a total field F(x, y, 0).

$$F(x, y - h) = \frac{h}{2\pi}\iint \frac{F(x,y,0)\delta x \delta y}{(x-x')^2 + (y-y')^2 + h^2} \quad (3)$$

Equation 3 is the upward continuation equation that allows us to calculate magnetization anywhere in the free space from the knowledge of its values over the surface. The left side is the total field at the point P (x, y, -h) above the surface F(x, y, 0) on which it is known(Telford *et al.*, 1990).

Pseudo-Gravity Data Analysis

Not because a mass distribution genuinely matches the magnetic distribution beneath the magnetic source, but rather because gravity anomalies are more instructive and simpler to understand and measure than magnetic anomalies, pseudo-gravity transformation is helpful in the interpretation of magnetic anomalies (Blakely, 1995). The application of pseudo-gravity transform to magnetic data was originally done by Baranov (1957). This technique made it easy to eliminate the distortion brought on by the earth's magnetic field by shifting the magnetic anomalies' apex over the source body. Transformation techniques were used on the data to identify and delineate crustal magnetic sources, since magnetic anomalies are rarely centred above their origins. With Oasis Montaj version 7.0.1, the Fast Fourier Transform (FFT)

filter extension was utilised to apply the pseudo-gravity transform on the residual of the total magnetic intensity data.

Through pseudo-gravity transformation, a magnetic anomaly that was previously a dipole becomes a monopole and seems to be a gravitational anomaly (Subarsyah and Priohandono, 2016). This transformation is used to interpret magnetic anomalies since the outputs are similar to gravity data from a magnetic object with the density ratio. According to this translation, 1 A/m = 10^2 gamma, and 1 gamma ≈ 1 kg/m3. Therefore, the proportionality is 100 kg/m^3 for every A/m. according to Blakely (1995).

For a magnetized body, the magnetic potential V due to proportional density, and the gravitational potential, U can be related by the following Poisson' relation:

$$V = -\frac{C_m}{\gamma\rho} M\hat{m} \cdot \vec{\nabla} p_U \quad (4)$$

$$= \frac{-C_m M g_m}{\gamma\rho} \quad (5)$$

Where V is magnetic potential, U is gravitational potential, g_m is the component of gravity in the direction of magnetization, γ is Newton's constant, ρ is rock density (g/cm^3), C_m is magnetic constant, is magnetization (Am^{-1}). The assumption in this transformation is that M and ρ are constant, so the Fourier transform equation is (Subarsyah and Priohandono, 2016).

$$F[g_m] = \frac{\gamma}{C_m}\frac{\rho}{M} F[V] \quad (6)$$

Where,

$$F[V] = -\frac{1}{\theta_f|k|} F[\Delta T] \quad (7)$$

So that,

$$F[g_m] = -\frac{\gamma}{c_m \theta_f |k|}\frac{\rho}{M} F[\Delta T] \quad (8)$$

$$F_{(psg)} = -\frac{\gamma}{c_m \theta_f |k|}\frac{\rho}{M} \quad (9)$$

g_m in this case is pseudo-gravity.

Horizontal Gradient Magnitude (HGM)

A straightforward method for identifying linear structures from prospective field data, such as contacts and faults, is the horizontal gradient. According to Cordell and Grauch (1982), Cordell and Grauch (1985), the horizontal gradient magnitude HGM (x, y) for magnetic field M (x, y) is provided.

$$HGM(x,y) = \sqrt{\left(\frac{\delta M}{\delta x}\right)^2 + \left(\frac{\delta M}{\delta y}\right)^2} \quad (10)$$

Assuming the following, this function peaks over magnetic contacts: 1) the sources are thick, 2) the contact is vertical, and 3) the magnetic field and source magnetization are vertical. Peek shift away from the contact position results from breaking the first two assumptions Phillips (2000). Secondary peaks arise parallel to the contacts when the third assumption is broken. Using the approach on the regional component of the reduced to the equator magnetic data, a partial satisfaction of the first two assumptions was achieved. Upon reaching the equator, the majority of source magnetizations and the regional magnetic field will have a horizontal arrangement. Finding maxima in the HGM grid after a tiny 3' by 3' window is passed over it will reveal crests in the horizontal gradient magnitude grid. 1981 saw Blakely and Simpson. Lineaments that might correlate to basement faults and connections can be effectively detected by this method when certain assumptions are met.

RESULTS AND DISCUSSION

Surface Structural Trend Analysis of Lineaments

The remaining uncorrelated bands are blended into RGB, and the False Colour Composite (FCC) of bands 753 and 764 (Figure 2) developed models based on their correlation coefficient. The lithologies and alteration zones were mapped using these two colour composite models (Figure 2), which were created from Landsat-8 Mambilla and its surroundings. The textural characteristics of the outcrops allow them to be identified in the photograph from the background. The crystalline texture and structural features of the rocks in the image's area segment are clearly seen in the bands' natural RGB colour combination.

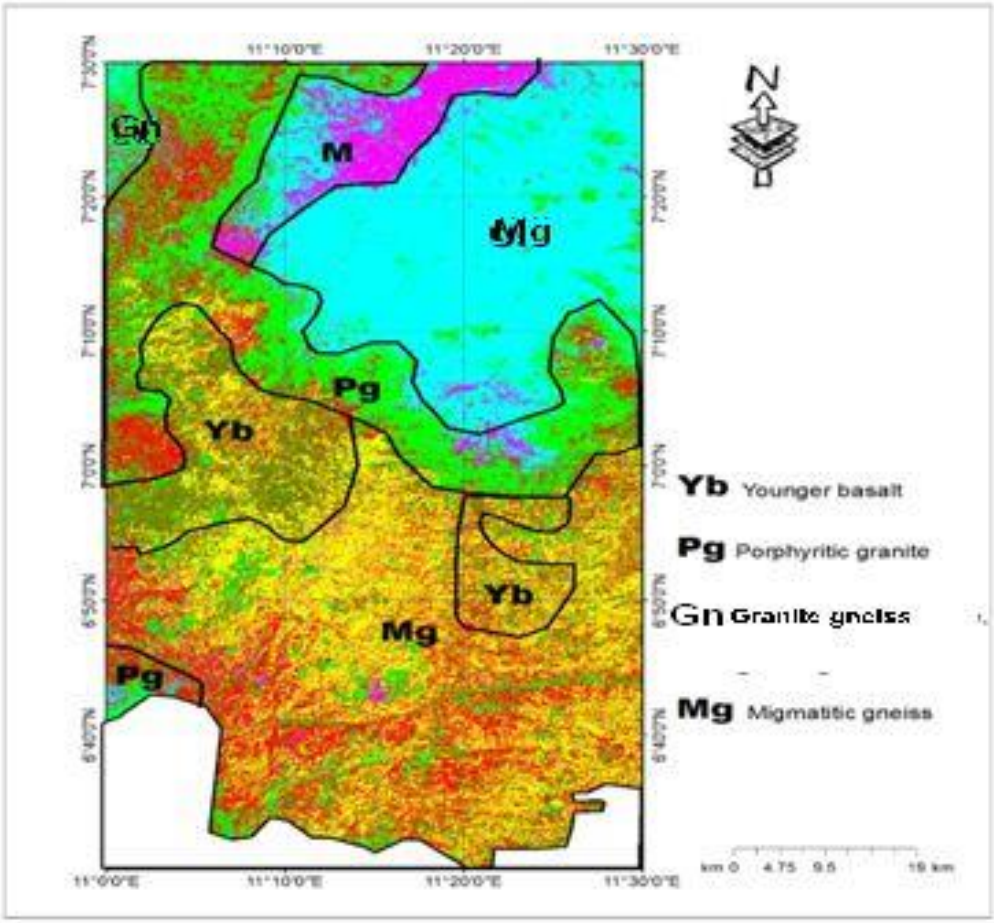

Figure 2: The false color composite image of Landsat-8 ETM+ (bands 7, 4, 2 in R, G, and B) shows the following rocks: migmatite-gneiss (Mg), granite gneiss (Gn), porphyritic granite (Pg), and younger basalt (Yb).

Principal Component analysis (PCA)

The PCA normalises the seven OLI bands and strengthens, compresses, and limits the leading bands. Each one was linearly improved to produce composite images (El-said *et al*., 2014). Bands 2456 and 716 were the PCAs employed in this investigation (Figure 3). As shown in Figure 3, the calculated statistical individual images and various data percentages were produced.Due to their bright pixels in PC2 of PCA 2456, which has a positive high reflectance

in band 6 (0.451293) and negative absorption in band 3 (-0.434848), the eigenvectors showed that the majority of the younger basalt, porphyritic granite, granite gneisses, and migmatite-gneisses could be distinguished from one another. On the other hand, dark pixels were indicative of undifferentiated granite, migmatite, and granite gneiss. The aforementioned rocks were also recognised as bright green, purple, yellowish, and pinkish pixels in the RGB composite of PCA 716 (Figure 3).

Bright pixels in PC2 were used to distinguish between the PC of 2456 of the younger basalt, porphyritic granite, and migmatite gneisses, despite the fact that the positive absorption eigenvector in band 6 (0.518572) and negative in band 4 (-0.959506) mapped dark pixels. This was after the band 5 negative eigenvector value reflectance and positive in band 4. According to the composite of the PCA 716 picture, the majority of the reddish and pinkish pixels correspond to the migmatite gneisses rocks in the research area.The research area's different rock types showed a good correlation with the Mambilla and surrounding area's geological map.

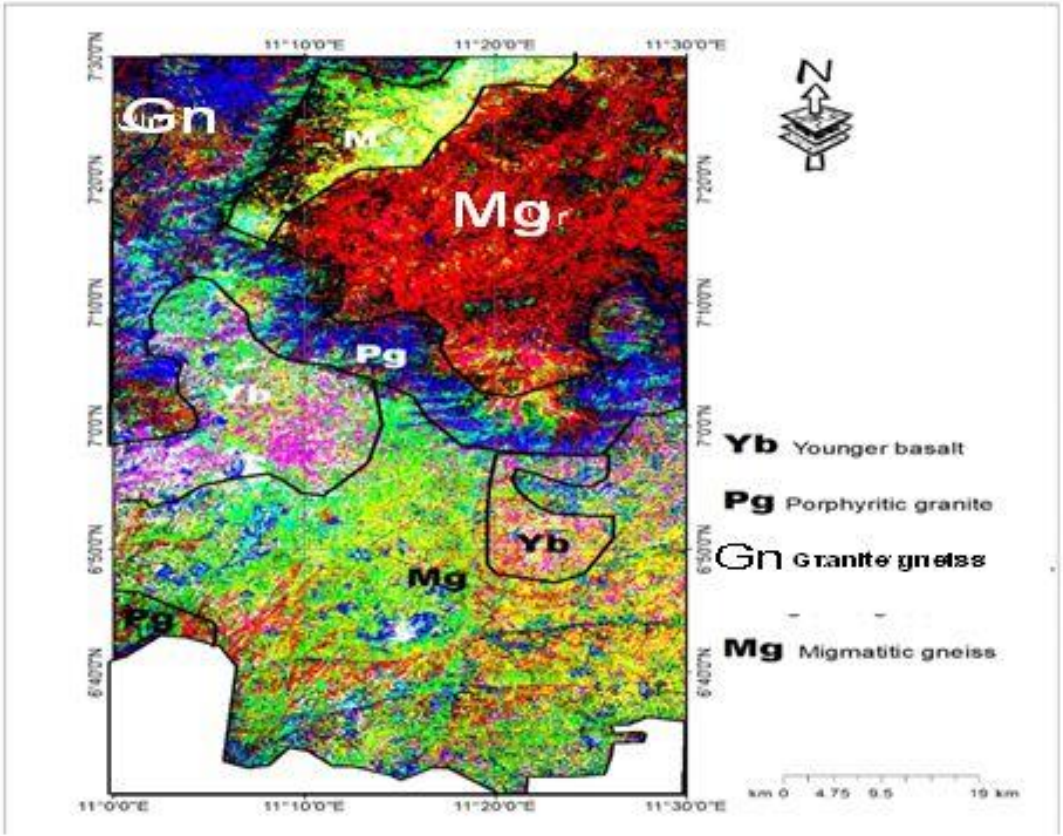

Figure 3: Principal component analysis of the study area's Landsat 8 ETM+ image (PC2, PC1, and PC4 in R, G, and B) identified the following rocks: migmatite-gneiss (Mg), granite gneiss (Gn), Porphyritic granite (Pg), and younger basalt (Yb).

Aeromagnetic data analysis

Total magnetic intensity (TMI), Crustal field and Reduction to equator (RTE)

Fugro gathered and stored the data in the following manner: X columns stand for longitude/easting, Y columns for latitude/northing, and Z columns for total magnetic intensity (TMI). In order to simplify processing, the aeromagnetic total field intensity value (Z) of 33,000 nT was removed. In order to obtain the Z-column total, a simple arithmetic addition of 33,000 nT to each value of the Z column had to be done after obtaining the data from NGSA before any further processing could be deemed legitimate. Once the Universal Transverse Mercator (UTM) projection method was used for georeferencing, X and Y were determined to be the ideal columns. The data gridding process ultimately produced the grid that represented the aeromagnetic total field strength in terms of colour images. The color-coded aeromagnetic total field intensity of the study area is shown in (Figure 4). The asymmetrical and low-data values associated with the structural features' NE-SW patterns and linear relationship to the southern half of the map are used to categorise them. With a deviation from mean of 31.50 and a mean of 33068.89nT, the lowest and maximum values for the gridded data were 33030.343nT and 33172.792nT, respectively. Over the region, the calculated geomagnetic inclination and declination range from -0.3^{o} to 7.2^{o} (mean: 3.5o) and -2.5o to -1.5o (mean: 0.24^{o}), respectively. The study location is clearly located in a low magnetic latitude region. The research region's southernmost section exhibited near-surface igneous rock possessing high magnetic susceptibility and magnetic intensity values.

The Total Magnetic Intensity (TMI) map over Mambilla and its surroundings displays an average value of 33078.888 nT, with TMI values ranging from 32892.772 nT to 33203.596 nT (Figure 4). High, low, and intermediate magnetic signals that can be attributed to rock susceptibility, depth to the source of magnetic rock, degree of strike, and remnant magnetism make up the resulting TMI map (Likkason, 2014). Among the villages with the highest TMI values were Gidan Garba, Maisamari, Gidan Godiya, Nguroje, Ngubio, Banga, Kakera, and Kilating. MajoTolore, NgelNyeki, Kuuku, Dan Fulani, Magu, Gidan Godiya, Mayo Juji, Bode Goje, Ida Manti, Mayo Selbe, Mayo Fundam, and Kara are among the areas where the Northeast-Southwest trends (Figure 4) are evident. These trends are the dominant trend and lineaments observable in the study area.

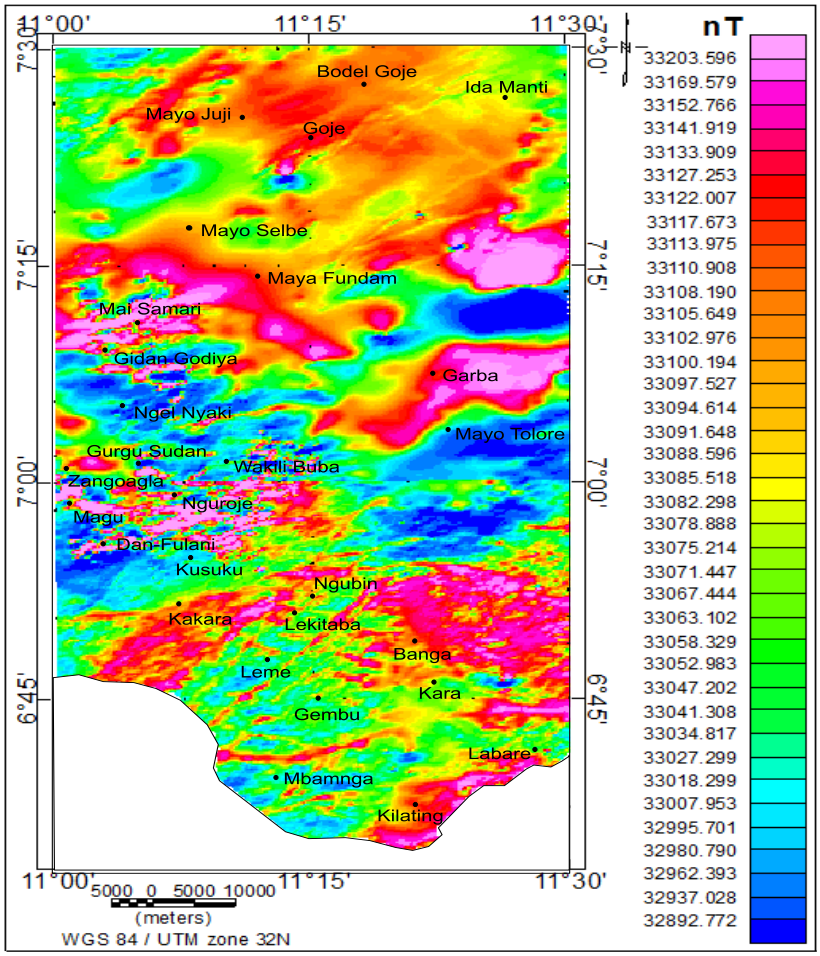

Figure 4: Aeromagnetic total field intensity map of Mambilla and environs

The values on the Main Magnetic field map over Mambilla and its surroundings range from 33228.522 nT to 33358.377 nT, with an average of 33293.4495 nT (Figure 5). This field is a representation of the research area's regional field that isn't on the (TMI) map. The villages Kilating, Kara, Leme, Dan Fulani, Mbanga, and Gembu, which trend NW-SE (Figure 5) and gradually grow from SW-NE, were found to have the lowest main fields.In addition, the main field rises from Ida Marti to Bode Goje; the highest main field was noted in the research area's far northeast. The NW-SW trend is the primary pattern for the entire main field (Figure.5).
The magnetic field of the crust was determined by deducting the measured magnetic field from the estimated magnetic field (Thompson, 1982). The 2005 DGRF model served as the basis for the magnetic field correction in this specific investigation.

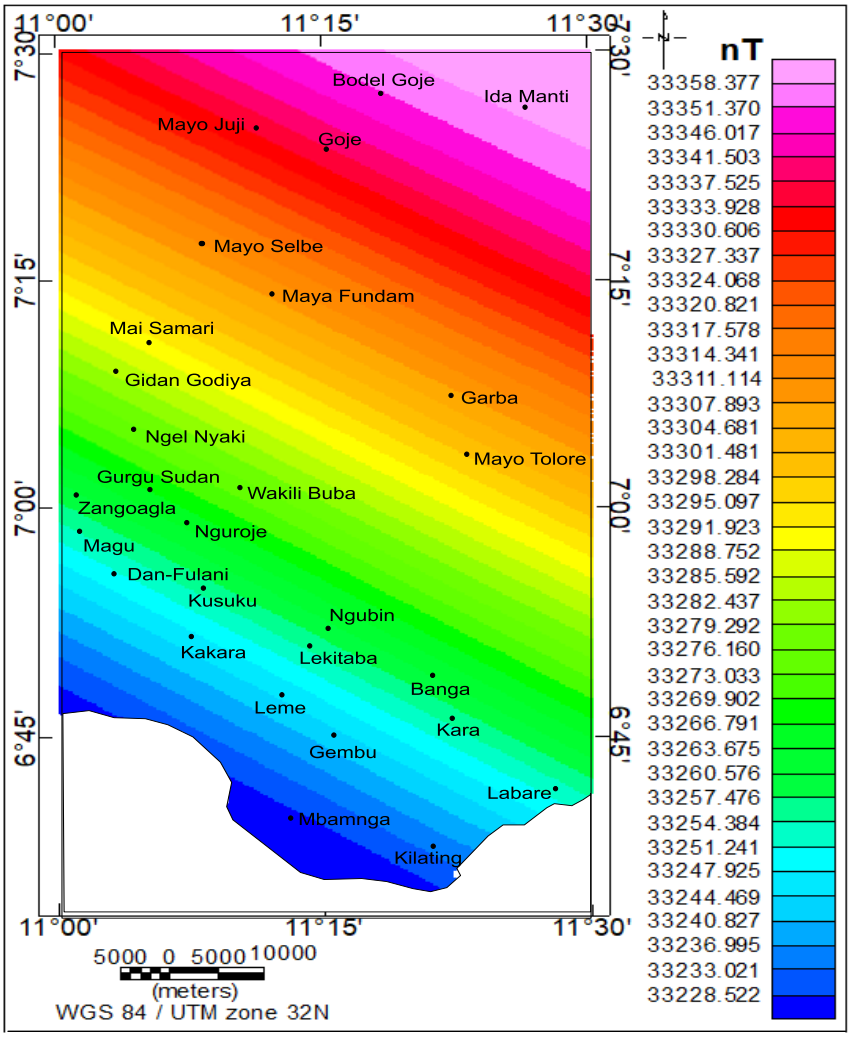

Figure 5: Map of Generated Geomagnetic main field of Mambilla and environs

The average value of the crustal magnetic field map over Mambilla and its surroundings is -159.50nT, with values ranging from -397.669nT to -80.699nT (Figure 6). Pyroxene, olivine, magnetite, ilmenite, plagioclase feldspar, and other minerals are among the many minerals found in basaltic rocks (Auckland, 2005). The high interval of the local magnetic anomaly value is thought to have been largely caused by the magnetite found in basaltic rocks. Differences in the geological, magnetic, and chemical compositions of the rock masses are indicated by variations in the crustal magnetic field within the study area. Whereas the pink-colored portions indicate strong magnetization, the blue-colored areas indicate low magnetization. As seen in Figure 6, areas with high magnetic values (pink colour) have magnetised entities that are shallow to near the surface. The migmatite-gneiss complexes are most likely exposed on the surface or may have been buried at relatively shallow depths, as indicated by the high magnetic anomalies found in the majority of the studied area. Conversely, regions with low magnetic values (blue hue) are caused by magnetic basement subsidence brought on by the epeirogenic uplift within the research area as well as deep-seated magnetised substances. As seen in (Figure.6), the values displayed by the study area's crustal field map are all negative, indicating a magnetic equatorial zone. The earth crustal field anomaly combines the unique impacts of mutually more extensive and deeper sources that are identified as local and regional sources and are regarded as noise. Consequently, residual anomalies are the anomalies of interest (Likkason, 2014).

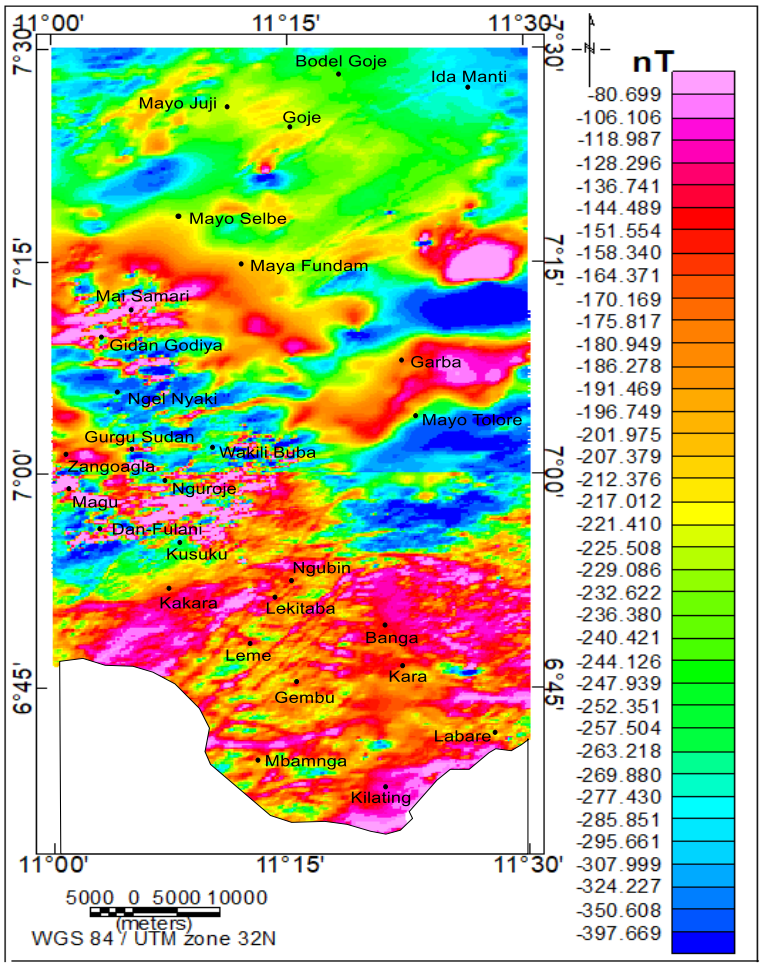

Figure 6: Crustal field (TMI) anomaly map of the study area

By centering the peaks' magnetic anomalies over their sources and augmenting the basement architecture, including structural lineaments with their orientations, the RTE map helps to eliminate the magnetic inclination effect in the low magnetic latitude zone. The magnetic strength variation over the research area led to the identification of two primary magnetic zones. Strong magnetic anomalies with amplitudes ranging from -82.382nT to -119.153nT predominate in the western, central, southern, and eastern regions (Figure.7). Nonetheless, the area's northern, northwest, and extreme southern regions are distinguished by relatively low amplitude magnetic intensity values (between -130.00nT and -392.122nT), which are indicated by greenish to blue colours and suggest regions with low magnetic content in their geological structures (fractures/faults).

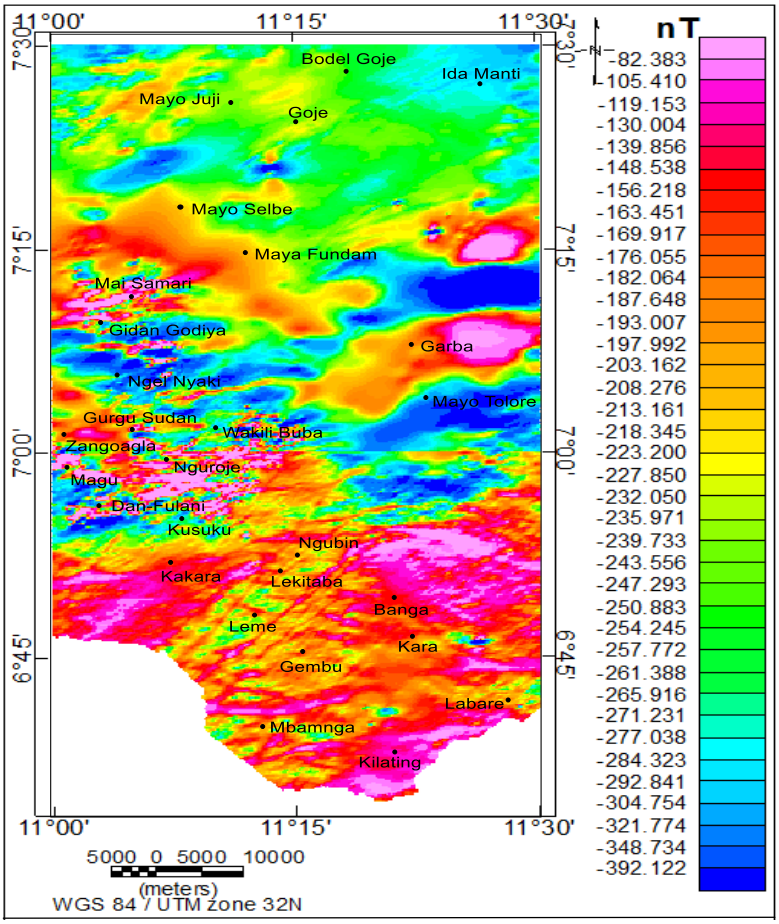

Figure 7: Reduction to equator map of Mambilla and Environs

Upward Continuation

Over Mambilla and its surroundings, the reduction to a magnetic equator field map was upward continued for 15 km, displaying values ranging from -279.141 nT to -157.160 nT. Compared to the crustal magnetic field in Figure 6, these upward continuing field levels are smaller. The areas of Mbanga, Gembu, and Kilating exhibit the strongest magnetic field, trending NW-SE (Figure 8). The magnetic field gradually decreases from NE-SW through May Tolore, followed by Bode Tolere, which likewise exhibits a NNE-SSE pattern. The NW-SE trend is the primary trend of the entire upward-trending field (Figure 8). The data on anomalies has been continuously collected upward until the anomaly contour pattern exhibits a generally steady or non-changing pattern (Ilapadila *et.al*. 2019). The magnetic anomaly contour map exhibits a smooth pattern at a height of 15 km, according to the analysis result of the anomalous contour pattern after upward continuation. Figure 8 displays the magnetic anomalous patterns that are the visual outcome of the upward continuation process starting at a height of 15 km.

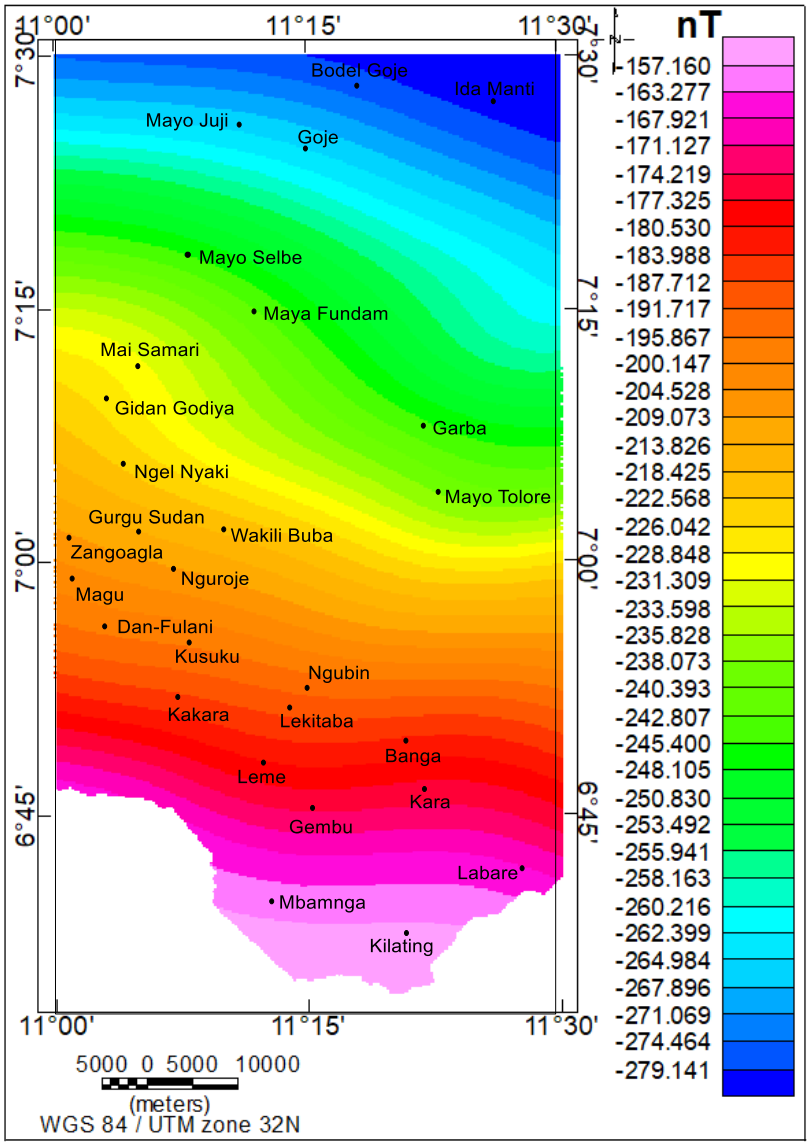

Figure 8: Upward Continuation ma at 15km of Mambilla and environs

Pseudo-Gravity Transformation

While the pseudogravity anomaly map (Figure 9) provides more information about the location of subsurface anomaly sources, horizontal gradient computations can be used to define the limits of lithological contacts. Pseudogravity anomaly data (Figure 9) emanating from subterranean objects or rocks tend to have a maximum horizontal gradient at their edge, which causes the maximum gradient to be localised just at the object's edge as Figure 10 illustrates (Blakely, 1995). By detecting the abrupt change in rock density in a lateral direction, this can be used to determine the contact boundaries between the surrounding rocks and the basaltic lithology (Nurdiyanto *et al.*, 2004). The region's pseudo-gravity map was split into three sections: high densities, ranging from 0.25 to 0.07 mg, intermediate densities, ranging from 0.06 to 0.01 mg, and low densities, ranging from -0.11 mg to -0.01 mg, respectively. The study area's pseudo-gravity map is displayed in Figure 9. As can be observed from the pseudogravity, landsat imagery, and geological maps, the comparatively high density areas are linked to basaltic intrusions because of the high densities of basalts. There is a significant density of rocks in the study area's middle and southernmost regions. Geological literature

(Asikin and Handoyo 1992) indicates that this is thought to be the centre of a very compact basaltic intrusion in the form of a dyke structure. While the low anomaly in the west, north, and east indicates the predominance of low density basement rocks near the surface, the high anomaly in the south and central sections shows the intrusion of compact basaltic rocks close to the surface. Daya1 *et al.* (2021) reported that bauxite deposits mineralized these locations. With values ranging from 0.003 to 0.553 mGal, the two bauxite-bearing hills at the Mayo Sumsum and Gurgu regions measure 500 m x 1000 m and 300 m × 1000 m, respectively. The distribution pattern of the basaltic intrusion in the region is represented by these lithological contact boundaries. Although there are some minor variations, the distribution pattern of basaltic rocks generally agrees with the geology, landsat imagery, and pseudogravity maps (Figures 1, 2, 3, and 9). This discrepancy makes sense as, according to Blakely (1995), the pseudogravity map illustrates the distribution pattern of basaltic intrusion both below and above the surface, but the geological map merely displays the distribution of basaltic rocks that are exposed at the surface. This basaltic rock not only penetrates from below but also intrudes the basement rocks. These rock units occur as sills and dyke structures in the field, which are intrusions with an elongated flat shape that are parallel and perpendicular to the plane of the rock strata (Sembiring *et al*., 2016).

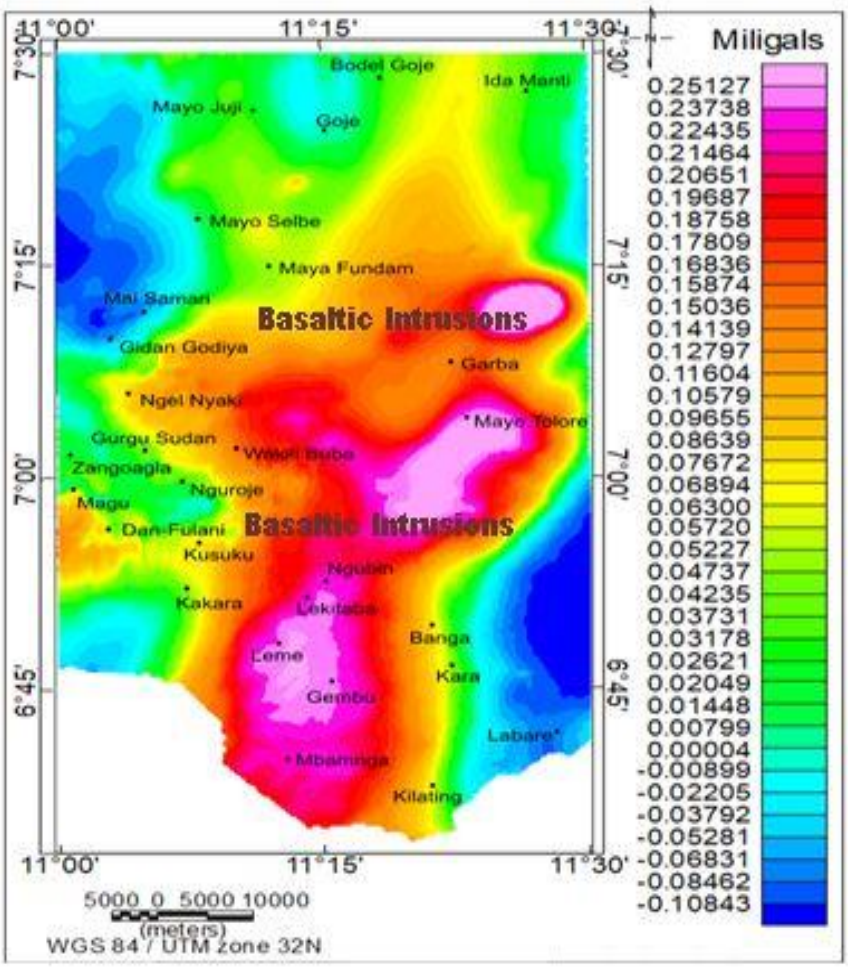

Figure 9: Pseudo-gravity transforms map of Mambilla and environs

Horizontal Derivatives (HDR)

Most of the structural components of the study field, including contacts, inferred faults, intrusions, and the form of some lithology to some extent, are shown in horizontal derivatives images (Okpoli and Akinbulejo, 2021). Horizontal gradient computations were applied to the RTE map in order to make the lithological contact boundaries more clear, even if the pseudogravity anomaly contour map is comparatively more useful in displaying the location of subsurface anomaly sources. The largest gradient will be localised precisely at the edge of the bodies since the maximum horizontal gradient of RTE anomaly data originating from subsurface rocks tends to be at the object's edge (Figure 10). By detecting the abrupt lateral variations in rock magnetism, this can be used to determine the contact boundaries between the surrounding rocks and the basaltic lithology (Nurdiyanto *et al.*, 2004). Figure 11 displays the contour of the horizontal gradient, with values ranging from 0.011 to - 0.11nT. In the research region, the distribution pattern of the basaltic intrusion is represented by these lithological contact boundaries. Although there are a few minor variations, the distribution pattern of basaltic rocks generally agrees with the geology, satellite imaging, and pseudogravity maps (Figures 1, 2, 3, 9, and 10). This discrepancy makes sense since the horizontal gradient map shows the surface and subsurface horizontal borders of basaltic intrusion (Blakely, 1995).

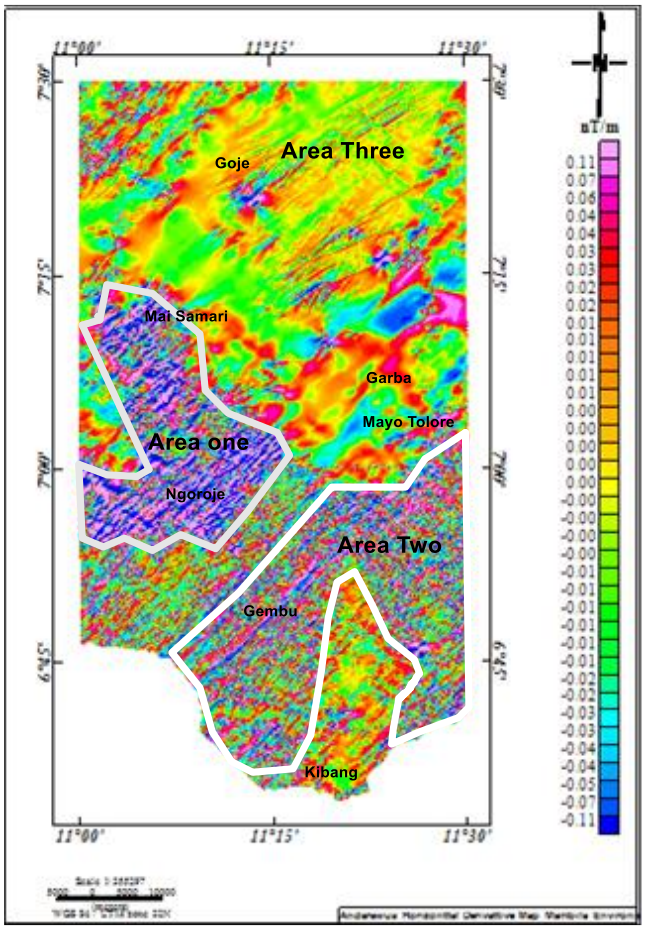

Figure 10: Horizontal derivative of magnetic data over Mambilla and environs

CONCLUSION

At the Mambilla Plateau and its surroundings, integrated geophysical analysis was used to pinpoint the position and patterns of basaltic intrusion. Whereas the principal component analysis of the Landsat 8 ETM+ image (PC2, PC1, PC4 in R, G, and B) of the study area identified rocks such as younger basalt (yb), porphyritic granite (pg), granite gneisses (Gn), and migmatite gneisses (Mg), the Landsat-8 ETM+ false colour composite image (bands 7, 4, 2 in R, G, and B) identified rocks such as these.Total magnetic intensity map a had minimum and maximum values of 33030.343nT and 33172.792nT, respectively, with a mean variation of 33068.89nT and 31.50nT. The average value of the main magnetic field map is 33293.4495 nT, with values ranging from 33228.522 nT to 33358.377 nT. The average value of the crustal magnetic field map, caused by localised ore bodies or intrusions, is -159.50 nT, with values ranging from -397.669 nT to -80.699 nT. The RTE values throughout the region range from -82.382nT to -392.122nT, indicating areas with faults, fractures, and geological intrusions. The magnetic equator field map was reduced and extended upward for a distance of 15 km, displaying values that varied between -279.141 nT and -157.160 nT. The area's pseudo-gravity map showed three distinct zones: low densities ranged from -0.11 to -0.01mGal, while high densities were found between 0.25mGal and 0.01mGal, indicating places with moderate to intermediate densities. The edge of the object is typically where the largest horizontal gradient of RTE anomalies data originating from subsurface rocks is found, allowing the maximum gradient to be directly localised to map boundaries of the distinct lithologies. This was used to determine the contact boundaries between the surrounding rocks and the basaltic intrusion, faults, mineralization, etc. by detecting the abrupt changes in rock magnetism in a lateral direction.

REFERENCES

Adagunodo, T. A., Sunmonu, L. A., and Adeniji, A. A., 2015. An Overview of Magnetic Method in Mineral Exploration, *Journal of Global Ecology and Environment*, vol. 3, no. 1, pp. 13-28,

Anonimous,Basalt((2020):Definition-Spread-Benefits,Available: https:// ilmugeografi .com/ geologi/batu-basalt, May 20, 2020.

Ansari and Alamdar,(2009). Reduction to the Pole of Magnetic Anomalies Using Analytic Signal, *World Applied Sciences Journal*, vol. 7, no. 4, pp. 405-409.

Asikin, S., and Handoyo, A., (1992). *Geological Map of Banyumas Sheet, Java, Scale 1: 100.000*. Center for Geological Research and Development, Bandung.

Baranov, V. (1957). A new Method for interpretation of Aeromagnetic Maps: Pseudo-gravimetric anomalies: Geophysics, Vol.22, pp 359–383.

Blakely, R.J. (1995). Potential Theory in Gravity and Magnetic Applications. Cambridge Univ. Press. 199, 464pp.

Cordell, L. and Grauch, V.J.S. (1982) Mapping Basement Magnetization Zones from Aeromagnetic Data in the San Juan Basin, New Mexico. SEG Technical Program Expanded Abstracts , 246-247.

Cyprian, B. M. (2012). *Iron Ore Mineral Deposits Exploration by Ground Magnetics in Kindani Area, Meru County, Kenya*. Thesis Master of Science, Physics Department Jomo Kenyatta, University of Science and Technology, Kenya,

Daya.A.M, Ahmad I. H, Maigari.A.S, and Yahuza.I (2021). Geology and Possible Host for Bauxite Mineralization of Mambila Plateau, NE Nigeria, International Journal of Geo-informatics and Geological Science, Volume 8 Issue 3, 22-28,

Eldosouky, A.M., (2019). Aeromagnetic data for mapping geologic contacts at Samr El- Qaa area, North Eastern Desert, Egypt. Arab. J. Geosci. 12, 2. https://doi.org/10.1007/s12517-018-4182-2.

Elkhateeb, S.O., Eldosouky, A.M., (2016). Detection of Porphyry Intrusions Using Analytic Signal (AS), Euler Deconvolution, and Center for Exploration Targeting (CET) Technique Porphyry Analysis at Wadi Allaqi Area, South Eastern Desert, Egypt. Int. J. Sci. Eng. Res. 7(6) pp. 471-477.

Farrand, W.H., Harsanyi, J.C., (1997). Mapping the distribution of mine tailings in the Coeur d'Alene River Valley, Idaho, through the use of a constrained energy minimization technique. Remote Sens. Environ. 59, 64–76.

Frantz C (1981). Development without communities: Social fields, Network and Action in the Mambilla Grasslands of Nigeria. J. Human org. pp. 211-220

Ganas, A., Pavlides, S., Karastathis, V., 2005. DEM-based morphometry of rangefront escarpments in Attica, central Greece, and its relation to fault slip rates. Geomorphology 65 (3-4), 301–319.

Geomatics(PCI) Enterprises Inc, 2015. geospatial image processing software. www.pcigeomatics.com..

Goetz, A.F.H., Rock, B.N., Rowan, L.C., 1983. Remote sensing for exploration: an overview, Econ. Geol. 78, 573-590.

Harsanyi, J.C.,(1993). Detection and classification of subpixel spectral signatures in hyperspectral image sequences Unpublished Ph.D. Thesis. University of Maryland, p. 116.

Ilapadila, Herimei, B., and Maria C(2019)..Analysis of Regional Anomaly on Magnetic Data Using the Upward Continuation Method, *The International Conference on Geoscience*, *IOP Conference Series*: *Earth and Environmental Science* 279.

Jeje L.K (1983). Aspects of geomorphology of Nigeria. Heinemann educational books.

Likkason. O. K (2014). Exploring and Using the Magnetic Methods. http://dx.doi.org/10.5772/57163

Lino, L. M., Cavallaro, F. A., Vlach, S. R. F., and Coelho, D. C. (2018). 2D Magnetometric Modeling of a Basic-Intermediate Intrusion Geometry: Geophysical and Geological Approaches Applied to The Limeira Intrusion, Paraná Magmatic Province (SP, Brazil), *Brazilian Journal of Geology*, vol. 48, no. 2, pp. 305-315.

Mould .A.W. S (1960). Report on a rapid reconnaissance soil survey of the Mambilla plateau. Bulletin 15, Soil survey section, regional research station, ministry of agriculture, Samaru, Zaria.

Mubi AM, Tukur. A.L (2005). Geology and relief of Nigeria. Nigeria. Heinemann educational books.

Nikolakopoulos, K.G., Kamaratakis, E.K., Chrysoulakis, N., (2006). SRTM vs ASTER elevation products. Comparison for two regions in crete, Greece. Int. J. Remote Sens.. 27 (21), 4819–4838

Nurdiyanto, B. S., Wahyudi, Suyanto, I., Magnetic Data Analysis to Determine the Subsurface Structure of the Hot Water Manifestation Area on the North Slope of Ungaran Volcano, *Proceedings of the Indonesian Geophysicists Association*, 29th Annual Scientific Meeting, Yogyakarta, October 5-7, 2004.

Okpoli, C.C., Eyitoyo, F.B., (2016). Aeromagnetic study of Okitipupa region. Southwestern Nigeria, International Basic and Applied Research Journal 2 (7), 1–20.

Okpoli, C.C., Akinbulejo, B.O., (202). Aeromagnetic and electrical resistivity mapping of groundwater development around Ilesha schist belt, southwestern Nigeria. J. Pet. Explor. Prod. Pp15

Poormirzaee, R., Oskouei, M.M., (2010). Use of spectral analysis for detection of alterations in ETM data, Yazd, Iran. Appl. Geomatica 2 (4), 147–154.

Pour, A.B., and Hashim, M., (2016). Geological features mapping using PALSAR-2 data in Kelantan River Basin, Peninsular Malaysia. The International Archives of the Photogrammetry, Remote Sensing and Spatial Information Sciences, Volume XLII-4/W1, 2016 International Conference on Geomatic and Geospatial Technology (GGT), Kuala Lumpur, Malaysia. doi: 10.5194/isprs-archives-XLII-4-W1-65-2016

Pour, A.B., Hashim, M., Hong, J.K., Park, Y., (2019). Lithological and alteration mineral mapping in poorly exposed lithologies using Landsat-8 and ASTER satellite data: north-eastern Graham Land, Antarctic Peninsula. Ore Geol. Rev. 108, 112–133.Ramadan.

Phillips, J.D. (2000) Locating Magnetic Contacts: A Comparison of the Horizontal Gradient, Analytic Signal, and Local Wavenumber Methods: Society of Exploration Geophysicists. Abstracts with Programs, Calgary, 2000.

Roy, D.P., Wulder, M.A., Loveland, T.R., C.E., W., Allen, R.G., Anderson, M.C., Helder, D., Irons, J.R., Johnson, D.M., Kennedy, R., Scambos, T.A., Schaaf, C.B., Schott, J.R.Sheng, Y., Vermote, E.F., Belward, A.S., Bindschadler, R., Cohen, W.B., Gao, F., Hipple, Hostert, P., Huntington, J., Justice, C.O., Kilic, A., Kovalskyy, V., Lee, Z.P., Lymburner, L., Masek, J.G., McCorkel, J., Shuai, Y., Trezza, R., Vogelmann, J., Wynne, R.H., Zhu, Z., 1998. Landsat-8: Science and product vision for terrestrial global change research. Remote Sens. Environ. 145, 154–172.

Sembiring, R.R., Sunarwan, B., Syaiful, M., (2016). Geology and Study of Turbidite Deposits in Ciwuni and Surrounding Areas, Kesugihan District, Cilacap Regency, Central Java, *Jurnal Online Mahasiswa* (JOM) *Geological Engineering Section*, vol. 1, no. 1, pp. 1-14.

Süzen, M.L., Toprak, V., (1998). Filtering of satellite images in geological lineament analyses: an application to a fault zone in Central Turkey. Int. J. Remote Sens. 19(6), 1101–1114.

Subarsyah S and Priohandono YA 2016 Metoda Pseudo-Gravity DalamAnalisisKelurusan Dan Patahan Di SekitarTinggianAsahan, PerairanSelatMalaka. *J GeolKelaut***7(2)** p.65–71

Tanaka, A., Okubo, Y. and Matsubayashi, O.(1999). Curie point depth based on spectrum analysis of the magnetic anomaly data in east and southeast Asia. Tectonophysics 306, 461-470.

Telford, W. M., Gedaart, L. P, Sheriff, R. E.,(1990). *Applied Geophysics*, Cambridge University Press, Cambridge.

The University of Auckland(2019). Geology Rock and Mineral; Basalt, Available: https://flexiblelearning.auckland.ac. nz/rocks_minerals/rocks/basalt.html, November 17..

Thomson, D.J. (1982) Spectrum Estimation and Harmonic Analysis. Proceedings of the IEEE, 70, 1055-1096. https://doi.org/10.1109/PROC.1982.12433

Tukur, A. L, Adebayo. A. A, Galtima A (2005). The land and people of the Mambilla Plateau, Nigeria. Heinemann educational.

Udensi, E. E., Osazuwa I. B. and Daniyan, M. A. (2003). Trend analysis of the total magnetic field over the Bida Basin, Nigeria. Nigerian Journal of Physics. 15,143–151.